AIAA JOURNAL
Vol. 31, No. 8, August 1993

Comparison of Two-Equation Turbulence Models for Boundary Layers with Pressure Gradient

David C. Wilcox*
DCW Industries, Inc., La Cañada, California 91011

This paper compares the performance of eight low Reynolds number k-ϵ and k-ω models for high Reynolds number, incompressible, turbulent boundary layers with favorable, zero, and adverse pressure gradients. Results obtained underscore the k-ϵ model's unsuitability for such flows. Even more seriously, the k-ϵ model is demonstrated to be inconsistent with the well-established physical structure of the turbulent boundary layer, and low Reynolds number corrections cannot remove the inconsistency. By contrast, the k-ω model, with and without low Reynolds number modifications, proves to be very accurate for all of the tests conducted.

I. Introduction

MOST of the turbulence model community uses the well-known k-ϵ model[1,2] as the foundation for complex turbulent-flow applications in which turbulence scales are unknown a priori. As early as 1977, Chambers and Wilcox[3] raised questions about the wisdom of the model's widespread use by demonstrating two serious flaws for wall-bounded flows. First, they showed that the model is very ill behaved approaching a solid boundary, which precludes straightforward integration through the viscous sublayer. Many researchers have indeed found that its equations can be integrated through the viscous sublayer only with the aid of complicated viscous damping functions that make the equations very stiff. Second, they demonstrated an even more objectionable feature of the model, namely, that it is very inaccurate for flows with adverse pressure gradient. These predictions were borne out at the 1980–81 AFOSR-HTTM-Stanford Conference on Complex Turbulent Flows,[4] where the model failed to accurately predict many adverse pressure gradient flows. Rodi and Scheuerer[5] confirmed the model's problems in adverse pressure gradient and proposed what proved to be an unsatisfactory solution. Using singular perturbation methods, Wilcox[6] has explained the k-ϵ model's deficiency. He demonstrated that 1) the k-ϵ model's defect-layer structure is consistent with measurements only for constant-pressure turbulent boundary layers and that 2) wall functions, which are usually blamed for discrepancies between k-ϵ model predictions and measurements, play only a minor role.

By contrast, the Wilcox k-ω model has neither of these deficiencies. Many applications have been made that show that 1) the k-ω model's defect-layer structure is consistent with measurements of turbulent boundary layers for all pressure gradients from favorable to strong adverse and that 2) the k-ω model can be integrated through the viscous sublayer without the aid of viscous damping functions (this cannot even be done with an algebraic model!). The model is as accurate using wall functions as it is when integrated through the sublayer.

There is a popular misconception that low Reynolds number modifications to the k-ϵ model can remove its deficiencies for adverse pressure gradient flows. This mistaken notion overlooks the volumes of data on and physical understanding of turbulent boundary layers established during the 20th century, most notably by Clauser and Coles.[12] Specifically, Coles[7] describes the turbulent boundary layer as a "wake-like structure constrained by a wall" and notes that different scales and physical processes are dominant in the sublayer and defect layer. As just noted, Wilcox has shown that the k-ω model is consistent with observed defect-layer structure, whereas the k-ϵ model is not. Hence, we cannot reasonably expect viscous corrections (which are negligible in the physical defect layer) to correct the inconsistency.

Some controversy remains regarding the universality of the defect-layer analysis of Wilcox, which is strictly valid only for equilibrium turbulent boundary layers. Equilibrium in this context means the so-called equilibrium parameter β_T defined by

$$\beta_T = \frac{\delta^*}{\tau_w}\frac{dp}{dx} \tag{1}$$

is constant, where δ^* is displacement thickness, τ_w is surface shear stress, and dp/dx is pressure gradient. The possibility exists that the equilibrium turbulent boundary layer is a pathological case and the perturbation analysis lacks sufficient generality to warrant conclusions pertaining to nonequilibrium boundary layers. The purpose of this paper is to remove all doubt that an insufficient number of tests of the k-ϵ model have been made for nonequilibrium adverse pressure gradient flows to demonstrate the validity of Wilcox's analysis. To accomplish this end, we apply six low Reynolds number variants of the model to 16 incompressible, two-dimensional boundary layers with pressure gradients ranging from favorable to strongly adverse. We also apply low and high Reynolds number versions of the k-ω model to these flows.

Sections II and III identify the models and flows selected for the comparisons. Section IV compares computed and measured skin friction for the 16 cases. Section V illustrates the consistency of Wilcox's defect-layer analysis with numerical results for both k-ϵ and k-ω models. Section VI summarizes results of the study.

II. Models Selected

All computations in this study have been done using six low Reynolds number variants of the k-ϵ model and two versions of the k-ω model. Table 1 lists the models used with appropriate references. The k-ω model denoted by WH is the high Reynolds number version of the model. It includes viscous effects only through introduction of standard molecular diffusion terms. By contrast, the k-ω model denoted by WL is the low Reynolds number version formulated by Wilcox[7] specifically for transitional flows.

Received Oct. 16, 1992; revision received Feb. 1, 1993; accepted for publication Feb. 8, 1993. Copyright © 1993 by the American Institute of Aeronautics and Astronautics, Inc. All rights reserved.

*President, 5354 Palm Drive. Associate Fellow AIAA.

Table 1 Turbulence models

Identity	Type	Reference
JL	k-ϵ	Jones and Launder[1]
LS	k-ϵ	Launder and Sharma[2]
LB	k-ϵ	Lam and Bremhorst[9]
CH	k-ϵ	Chien[10]
YS	k-ϵ	Yang and Shih[11]
FL	k-ϵ	Fan et al.[12]
WH	k-ω	Wilcox[6]
WL	k-ω	Wilcox[8]

A. Mean-Flow Equations

The Reynolds-averaged equations for conservation of mass and momentum are the same for all models. The equations for incompressible boundary layers are as follows:

$$\frac{\partial u}{\partial x}+\frac{\partial v}{\partial y}=0 \tag{2}$$

$$u\frac{\partial u}{\partial x}+v\frac{\partial v}{\partial y}=-\frac{1}{\rho}\frac{dp}{dx}+\frac{\partial}{\partial y}\left[(\nu+\nu_T)\frac{\partial u}{\partial y}\right] \tag{3}$$

In Eqs. (2) and (3), x and y are streamwise and normal distances, u and v are streamwise and normal velocity components, ρ and p are fluid density and pressure, and ν and ν_T are molecular and eddy viscosity.

B. k-ω Model Equations

For the k-ω model the eddy viscosity is given by

$$\nu_T=\alpha^* k/\omega \tag{4}$$

where k is turbulence kinetic energy, ω is specific dissipation rate, and α^* is a closure coefficient. The equations for k and ω applicable to incompressible boundary layers are as follows:

$$u\frac{\partial k}{\partial x}+v\frac{\partial k}{\partial y}=\nu_T\left(\frac{\partial u}{\partial y}\right)^2-\beta^*\omega k+\frac{\partial}{\partial y}\left[(\nu+\sigma^*\nu_T)\frac{\partial k}{\partial y}\right] \tag{5}$$

$$u\frac{\partial \omega}{\partial x}+v\frac{\partial \omega}{\partial y}=\alpha\frac{\omega}{k}\nu_T\left(\frac{\partial u}{\partial y}\right)^2-\beta\omega^2+\frac{\partial}{\partial y}\left[(\nu+\sigma\nu_T)\frac{\partial \omega}{\partial y}\right] \tag{6}$$

The closure coefficients α^*, α, β^*, β, σ^*, and σ for the two versions of the k-ω model are as follows.

WH: high Reynolds number Wilcox model:

$$\alpha^*=1,\quad \alpha=5/9,\quad \beta^*=9/100,\quad \beta=3/40$$
$$\sigma^*=1/2,\quad \sigma=1/2 \tag{7}$$

WL: low Reynolds number Wilcox model:

$$\alpha^*=\frac{\alpha_0^*+Re_T/R_k}{1+Re_T/R_k}$$

$$\alpha=\frac{5}{9}\cdot\frac{\alpha_0+Re_T/R_\omega}{1+Re_T/R_\omega}\cdot(\alpha^*)^{-1}$$

$$\beta^*=\frac{9}{100}\cdot\frac{5/18+(Re_T/R_\beta)^4}{1+(Re_T/R_\beta)^4} \tag{8}$$

$$\beta=3/40,\quad \sigma^*=1/2,\quad \sigma=1/2,\quad \alpha_0^*=\beta/3$$

$$\alpha_0=1/10,\quad R_\beta=8,\quad R_k=6,\quad R_\omega=27/10$$

and Re_T is turbulence Reynolds number defined by

$$Re_T=\frac{k}{\omega\nu} \tag{9}$$

C. k-ϵ Model Equations

For the k-ϵ model the eddy viscosity is

$$\nu_T=C_\mu f_\mu k^2/\tilde{\epsilon} \tag{10}$$

and the equations for k and $\tilde{\epsilon}$ are

$$u\frac{\partial k}{\partial x}+v\frac{\partial k}{\partial y}=\nu_T\left(\frac{\partial u}{\partial y}\right)^2-\epsilon+\frac{\partial}{\partial y}\left[(\nu+\nu_T/\sigma_k)\frac{\partial k}{\partial y}\right] \tag{11}$$

$$u\frac{\partial \tilde{\epsilon}}{\partial x}+v\frac{\partial \tilde{\epsilon}}{\partial y}=f_1 C_{\epsilon 1}\frac{\tilde{\epsilon}}{k}\nu_T\left(\frac{\partial u}{\partial y}\right)^2-f_2 C_{\epsilon 2}\frac{\tilde{\epsilon}^2}{k}+E+\frac{\partial}{\partial y}\left[(\nu+\nu_T/\sigma_\epsilon)\frac{\partial \tilde{\epsilon}}{\partial y}\right] \tag{12}$$

where the dissipation ϵ is defined by

$$\epsilon=\tilde{\epsilon}+\epsilon_0 \tag{13}$$

The six low Reynolds number versions of the k-ϵ model considered in this study differ in the form of the damping functions f_μ, f_1, f_2, ϵ_0, and E; in the values of the closure coefficients; and in the surface boundary condition imposed on $\tilde{\epsilon}$. The damping functions depend on one or more of the following three dimensionless parameters:

$$Re_T=\frac{k^2}{\tilde{\epsilon}\nu},\quad R_y=\frac{k^{1/2}y}{\nu},\quad y^+=\frac{u_\tau y}{\nu} \tag{14}$$

The damping functions, closure coefficients and surface boundary condition on ϵ for the six models are as follows:

JL: Jones-Launder model:

$$f_\mu=\exp\left[-2.5/(1+Re_T/50)\right]$$
$$f_1=1$$
$$f_2=1-0.3e^{-Re_T^2}$$
$$\epsilon_0=2\nu\left(\frac{\partial\sqrt{k}}{\partial y}\right)^2 \tag{15}$$
$$E=2\nu\nu_T\left(\frac{\partial^2 u}{\partial y^2}\right)^2$$

$$C_{\epsilon 1}=1.45,\quad C_{\epsilon 2}=2.00,\quad C_\mu=0.09,\quad \sigma_k=1.0\quad \sigma_\epsilon=1.3$$
$$\tilde{\epsilon}=0\quad \text{at}\quad y=0$$

LS: Launder-Sharma model

$$f_\mu=\exp[-3.4/(1+Re_T/50)^2]$$
$$f_1=1$$
$$f_2=1-0.3e^{-Re_T^2}$$
$$\epsilon_0=2\nu\left(\frac{\partial\sqrt{k}}{\partial y}\right)^2 \tag{16}$$
$$E=2\nu\nu_T\left(\frac{\partial^2 u}{\partial y^2}\right)^2$$

$$C_{\epsilon 1}=1.44,\quad C_{\epsilon 2}=1.92,\quad C_\mu=0.09,\quad \sigma_k=1.0\quad \sigma_\epsilon=1.3$$
$$\tilde{\epsilon}=0\quad \text{at}\quad y=0$$

LB: Lam-Bremhorst model:

$$f_\mu = (1 - e^{-0.0165R_y})^2(1 + 20.5/Re_T)$$
$$f_1 = 1 + (0.05/f_\mu)^3$$
$$f_2 = 1 - e^{-Re_T^2} \tag{17}$$
$$\epsilon_0 = 0$$
$$E = 0$$
$$C_{\epsilon 1} = 1.44, \quad C_{\epsilon 2} = 1.92, \quad C_\mu = 0.09, \quad \sigma_k = 1.0 \quad \sigma_\epsilon = 1.3$$
$$\tilde{\epsilon} = \nu \frac{\partial^2 k}{\partial y^2} \quad \text{at} \quad y = 0$$

CH: Chien model:

$$f_\mu = 1 - e^{-0.0115y^+}$$
$$f_1 = 1$$
$$f_2 = 1 - 0.22e^{-(Re_T/6)^2} \tag{18}$$
$$\epsilon_0 = 2\nu \frac{k}{y^2}$$
$$E = -2\nu \frac{\tilde{\epsilon}}{y^2} e^{-y^+/2}$$
$$C_{\epsilon 1} = 1.35, \quad C_{\epsilon 2} = 1.80, \quad C_\mu = 0.09, \quad \sigma_k = 1.0 \quad \sigma_\epsilon = 1.3$$
$$\tilde{\epsilon} = 0 \quad \text{at} \quad y = 0$$

YS: Yang-Shih model:

$$f_\mu = \frac{[1 - \exp(-1.5 \cdot 10^{-4}R_y - 5 \cdot 10^{-7}R_y^3 - 10^{-10}R_y^5)]^{1/2}}{(1 + 1/\sqrt{Re_T})}$$
$$f_1 = \sqrt{Re_T}/(1 + \sqrt{Re_T})$$
$$f_2 = \sqrt{Re_T}/(1 + \sqrt{Re_T})$$
$$\epsilon_0 = 0 \tag{19}$$
$$E = \nu\nu_T\left(\frac{\partial^2 u}{\partial y^2}\right)^2$$
$$C_{\epsilon 1} = 1.44, \quad C_{\epsilon 2} = 1.92, \quad C_\mu = 0.09, \quad \sigma_k = 1.0, \quad \sigma_\epsilon = 1.3$$
$$\tilde{\epsilon} = 2\nu\left(\frac{\partial\sqrt{k}}{\partial y}\right)^2 \quad \text{at} \quad y = 0$$

FL: Fan et al. model:

$$f_\mu = 0.4\frac{f_w}{\sqrt{Re_T}} + \left(1 - 0.4\frac{f_w}{\sqrt{Re_T}}\right)(1 - e^{-Ry/42.63})^3$$
$$f_1 = 1$$
$$f_2 = [1 - 0.22e^{-(Re_T/6)^2}]f_w^2 \tag{20}$$
$$f_w = 1 - \exp\left[-\frac{\sqrt{R_y}}{2.30} + \left(\frac{\sqrt{R_y}}{2.30} - \frac{R_y}{8.89}\right)(1 - e^{-Ry/20})^3\right]$$
$$\epsilon_0 = 0$$
$$E = 0$$
$$C_{\epsilon 1} = 1.39, \quad C_{\epsilon 2} = 1.80, \quad C_\mu = 0.09, \quad \sigma_k = 1.0, \quad \sigma_\epsilon = 1.3$$
$$\frac{\partial\tilde{\epsilon}}{\partial y} = 0 \quad \text{at} \quad y = 0$$

III. Flows Selected

We have selected the best 15 cases (i.e., cases that satisfy the momentum integral equation) from the 1968 AFOSR-IFP-Stanford Conference[7] and one case from the 1980–81 AFOSR-HTTM-Stanford Conference on Complex Turbulent Flows.[4] Table 2 lists the flows. For flows 1100, 1200, 2100, and 5300 we omit data in regions where the momentum integral equation is out of balance by more than about 10%. Coles classified adverse pressure gradients as "mild," "moderate," and "strong" based on qualitative observations of velocity profile shape relative to the constant-pressure case and incipient separation. Inspection of the tabulated data for these flows shows that the strong adverse gradient cases have the largest local values of the equilibrium parameter β_T. We classify the single case from the 1980–81 conference (flow 0141) as having strong adverse pressure gradient because local values of β_T are comparable to those of flows 1200 and 4400.

IV. Results

All computations have been done with a two-dimensional boundary-layer program known as EDDYBL.[13] The program uses the Blottner[14] variable grid method augmented with an algorithm devised by Wilcox[15] to permit large streamwise steps. Program EDDYBL is second-order accurate in both streamwise and normal directions.

A grid resolution study has been conducted in which the number of grid points was varied from 60 to 250. Additionally, sensitivity to the location of the grid point closest to the surface was systematically evaluated for all eight models. In all cases, skin friction accurate to within 1.7, 0.4, and 0.1% can be obtained using 60, 100, and 200 grid points, respectively. The k-ω model displays virtually no sensitivity to the location of the point closest to the surface. Note that, as explained by Wilcox,[6,13] the exact solution for ω is specified at all points below $y^+ = 2.5$ to ensure numerical accuracy of the k-ω model solutions. Although the k-ϵ models display more sensitivity than k-ω, careful use of asymptotic limiting forms of the various damping functions near the wall alleviates most of the sensitivity. Nevertheless, using a value of the sublayer scaled normal distance, $y^+ < 0.1$, tends to slow convergence for most of the k-ϵ models.

All computations have been done using 100 grid points with point spacing increasing in a geometrical progression. The progression ratio is between 1.06 and 1.08 for all 16 cases. The average value of y^+ closest to the surface is 0.2. All computations have been initiated from approximated initial velocity, k and ϵ (or ω) profiles that guarantee a match to prescribed momentum and displacement thicknesses and to known asymptotic behavior of k, ϵ, and ω. Most of the computations require 50–100 streamwise steps and less than 20 s of CPU time on a 33 MHz 80486 microcomputer. Solutions with the

Table 2 Boundary-layer test cases

Flow	Type	Experimenter(s)
1400	Constant pressure	Wieghardt
1300	Favorable ∇p	Ludweig and Tillman
2700	Favorable ∇p	Herring and Norbury
6300	Favorable ∇p	Bauer
1100	Mild adverse ∇p ($x < 2.87$ m)	Ludweig and Tillman
2100	Mild adverse ∇p ($x < 20$ ft)	Schubauer and Klebanoff
2500	Mild adverse ∇p	Bradshaw
4800	Mild adverse ∇p	Schubauer and Spangenberg
2400	Moderate adverse ∇p	Bradshaw and Ferriss
2600	Moderate adverse ∇p	Bradshaw and Ferriss
3300	Moderate adverse ∇p	Bradshaw
4500	Moderate adverse ∇p	Schubauer and Spangenberg
0141	Strong adverse ∇p	Samuel and Joubert
1200	Strong adverse ∇p ($x < 2.87$ m)	Ludweig and Tillman
4400	Strong adverse ∇p	Schubauer and Spangenberg
5300	Strong adverse ∇p ($x < 4.1$ ft)	Stratford

k-ω model require about 30% less computing time than the various k-ϵ models.

The freestream values of k and ω (or ϵ) have been chosen to guarantee $\nu_T \ll \nu$ in the freestream. For the k-ω model, the freestream value of ω has a slight effect on computed C_f (less than 3% for all but flows 4500 and 4800 where increases in C_f as large as 10% occur for $\omega \to 0$). This is consistent with Menter's[16] observation that the k-ω model exhibits a small sensitivity to the freestream value of ω for boundary layers. The k-ϵ model shows no sensitivity to the freestream value of ϵ.

Favorable Pressure Gradient

Figure 1 compares computed and measured skin friction C_f for a constant pressure boundary layer (flow 1400) and for three cases with favorable pressure gradient (flows 1300, 2700, and 6300). As shown, the Jones-Launder (JL), Lam-Bremhorst (LB), and Yang-Shih (YS) models predict C_f values noticeably higher than corresponding measured values for the constant-pressure case. The Launder-Sharma (LS), Chien (CH) and Fan et al. (FL) models significantly underpredict skin friction in the early part of the flow 1300 computation. Overall, all of the k-ϵ models are within 10% (most are within 5%) of measured skin friction at the last streamwise station for all four flows. The k-ω model's skin friction virtually duplicates measured values at all stations for all four cases.

Mild Adverse Pressure Gradient

Figure 2 compares computed and measured skin friction for four cases with mild adverse pressure gradient (flows 1100, 2100, 2500, and 4800). For all but flow 2100, the k-ϵ models predict C_f values at least 25% higher than corresponding measured values. Interestingly, most of the k-ϵ models agree with measured skin friction for flow 2100. This case is an airfoil and has a very mild adverse pressure gradient up to the last station to which computations have been done. This explains why airfoil computations with the k-ϵ model are in reasonably good agreement with measurements, provided the angle of attack is not too large. As shown, the k-ω model, with and without low Reynolds number terms, predicts C_f values within 6% for all four cases.

Moderate Adverse Pressure Gradient

Figure 3 compares computed and measured skin friction for four cases with moderate adverse pressure gradient (flows 2400, 2600, 3300, and 4500). Even greater discrepancies (40% and larger) between computed and measured C_f exist for all of the k-ϵ models, whereas the k-ω models show no deterioration in predictive accuracy. Most of the k-ϵ models fortuitously match the experimental data at the end of the run for flow 2400, where the adverse gradient approaches zero.

Strong Adverse Pressure Gradient

Figure 4 compares computed and measured skin friction for four cases with strong adverse pressure gradient (flows 0141, 1200, 4400, and 5300). Differences between computed and measured C_f are in excess of 60% for all of the k-ϵ models for most of the flows. By contrast, C_f distributions predicted by the k-ω model are almost as close to measured values as in the preceding 12 applications. Note that Chien's model predicts boundary-layer separation very early in flow 5300, whereas all other k-ϵ models predict skin friction 300% higher than measured at the end of the run.

V. Discussion and Analysis

Table 3 provides a quantitative measure of the accuracy of the various models. The "errors" have been determined by first summing the absolute values of the differences between computed and measured C_f at the final station for the four cases in each flow category. Then the measured C_f values have been summed for the same four cases. The error is defined as the ratio of these two values. The overall average is the arithmetic mean of the errors for the four flow categories. Using

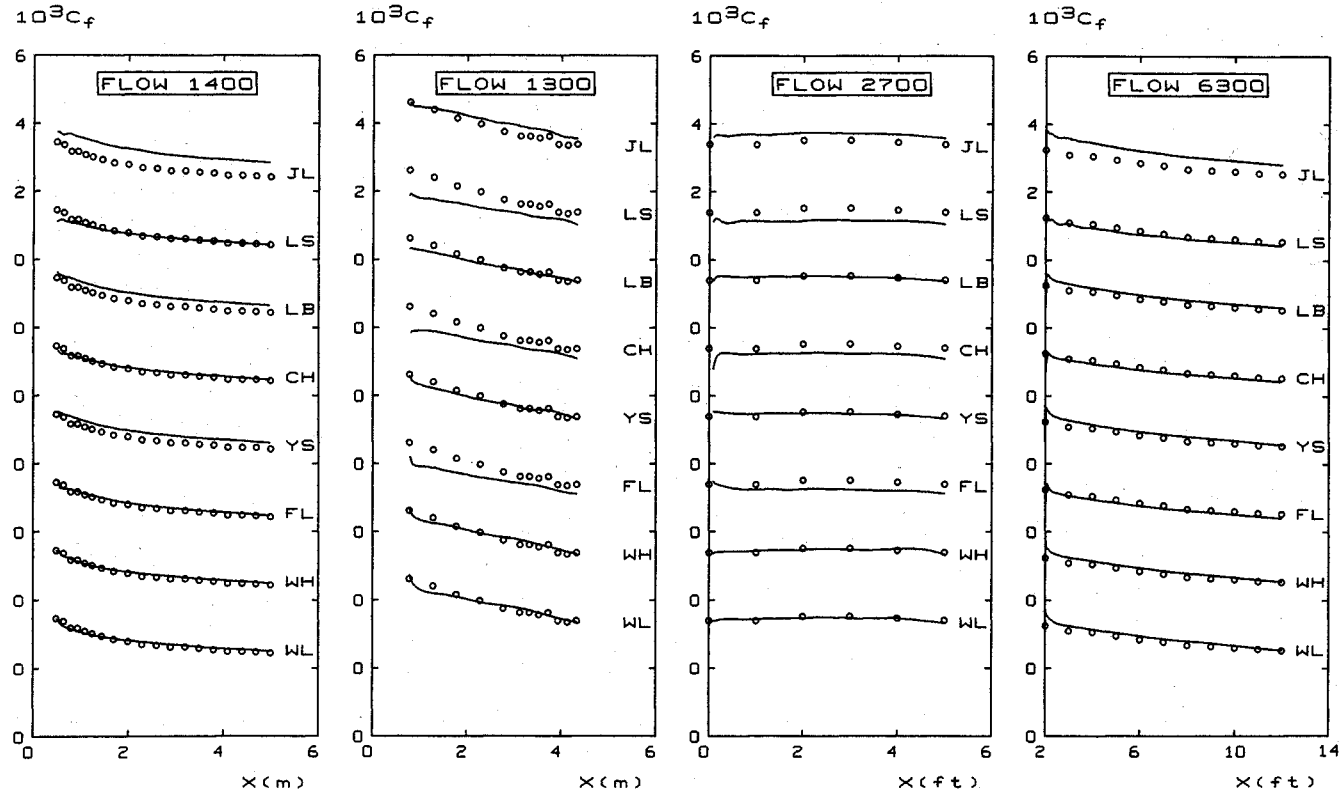

Fig. 1 Computed and measured skin friction; favorable pressure gradient.

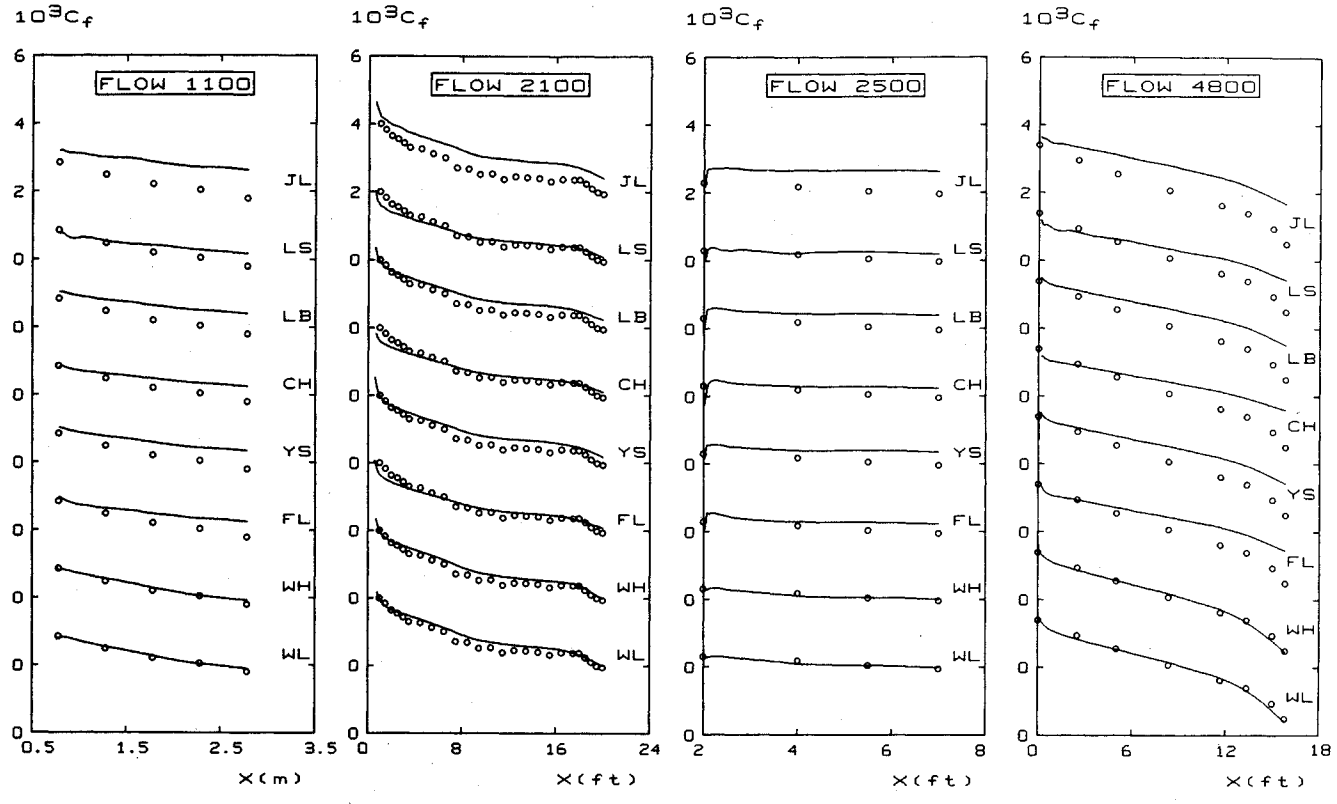

Fig. 2 Computed and measured skin friction; mild adverse pressure gradient.

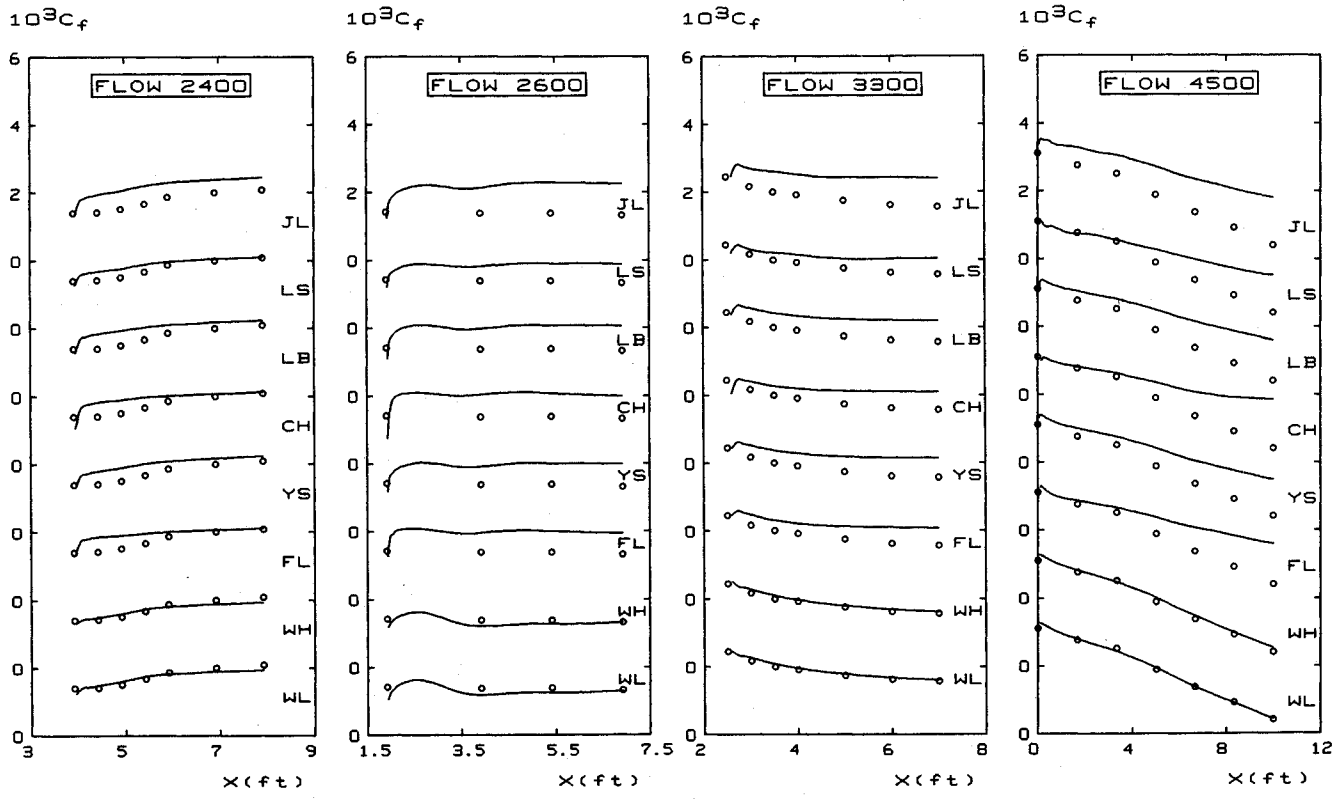

Fig. 3 Computed and measured skin friction; moderate adverse pressure gradient.

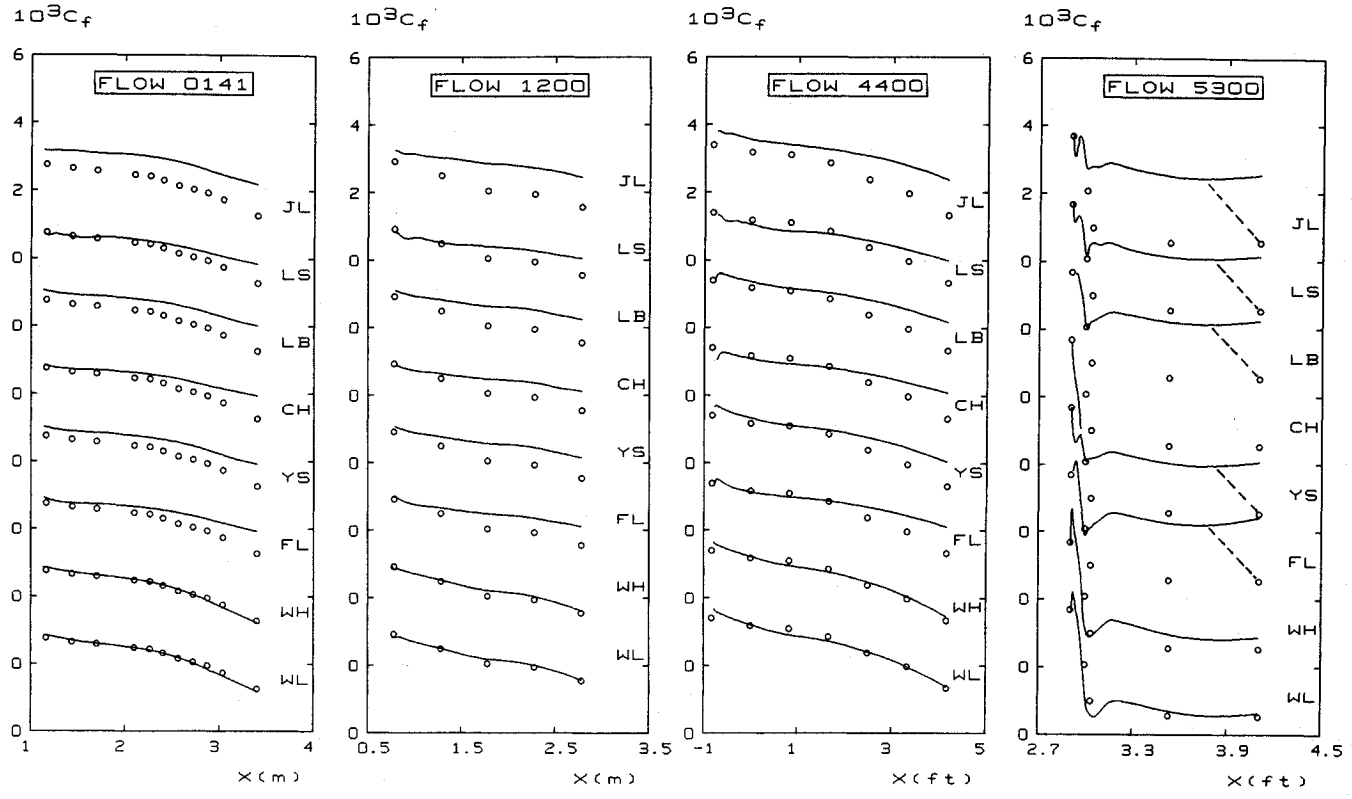

Fig. 4 Computed and measured skin friction; strong adverse pressure gradient.

Table 3 Percent error by flow type

Model	Favorable, %	Mild adverse, %	Moderate adverse, %	Strong adverse, %	Overall average, %
WL	2	4	4	6	4
WH	1	4	6	12	6
LS	7	27	40	71	36
CH	7	32	50	55	36
YS	3	34	46	75	40
FL	6	29	44	84	41
LB	3	38	50	85	44
JL	9	51	66	105	58

the skin friction at the last station is sensible since transients from approximate initial profiles have a minimal effect. Also, with the exception of flow 2400, the flows generally experience the strongest pressure gradient near the end of the computation. Since the 16 cases selected satisfy the momentum-integral equation to within 10%, the uncertainty in measured C_f can reasonably be estimated to be about 10%.

An interesting observation follows from inspection of the results presented in the preceding section and summarized in Table 3. Aside from the Jones-Launder model (which has been superseded by the Launder-Sharma model), there is little difference among the predictions of the k-ϵ models. Although we have not done computations using wall functions in this study, Wilcox[6] presents k-ϵ solutions obtained with wall functions that are nearly identical to the previous results for flows 1400, 3300, and 0141. Similarly, differences between k-ω model predictions with and without viscous corrections are slight. This indicates that precise details of the viscous damping functions have little effect (outside of the viscous sublayer) on model predictions for high Reynolds number boundary layers for both k-ϵ and k-ω models. This is unsurprising since it is the defect layer that responds most dramatically to changes in pressure gradient. In other words, the high Reynolds number version of a two-equation model dictates the response to pressure gradient regardless of the viscous damping terms implemented.

Wilcox[6] demonstrates this point for equilibrium boundary layers. Using singular-perturbation theory to analyze the defect layer, he shows that

$$\frac{U_e - u}{u_\tau} \sim -\frac{1}{\kappa}\ell n\eta + A - \beta_T C\eta\ell n\eta + \mathcal{O}(\eta^2\ell n\eta)$$

$$\text{as} \quad \eta \to 0 \tag{21}$$

where u, U_e, and u_τ are streamwise, freestream, and friction velocity, κ is von Kármán's constant, and A is a constant that must be determined from a numerical solution. The quantity β_T is given by Eq. (1), and η is the defect-layer coordinate, i.e.,

$$\eta = \frac{u_\tau}{U_e}\frac{y}{\delta^*} \tag{22}$$

where y is distance normal to the surface and δ^* is displacement thickness. Finally, the coefficient C is 2.90 for the k-ω model, whereas its value for the k-ϵ model is

$$C = \frac{(1 + \kappa^2/\sigma_k C_\mu^{1/2})C_{\epsilon 2} - C_{\epsilon 1}}{(2 - \kappa^2/\sigma_k C_\mu^{1/2})(C_{\epsilon 2} - C_{\epsilon 1})\kappa^2}$$

$$\text{where} \quad \kappa^2 = \sigma_\epsilon C_\mu^{1/2}(C_{\epsilon 2} - C_{\epsilon 1}) \tag{23}$$

All six k-ϵ models considered in this study use $C_\mu = 0.09$, $\sigma_k = 1.0$, and $\sigma_\epsilon = 1.3$. Table 4 summarizes the values of $C_{\epsilon 1}$, $C_{\epsilon 2}$, C, and κ for the various models tested. The most significant difference between the k-ω and k-ϵ velocity profiles is the magnitude of the coefficient C. It is nearly five times larger for the k-ϵ model. To see how this impacts model predictions, it is instructive to rewrite Eq. (21) in terms of sublayer coordi-

nates. Noting from Wilcox[6] that formal matching to the sublayer solution tells us

$$\frac{U_e}{u_\tau} = B + A + \frac{1}{\kappa}\ell n Re_{\delta^*} \tag{24}$$

where B is the usual constant in the law of the wall, Re_{δ^*} is the Reynolds number based on δ^*, and $\eta = y^+/Re_{\delta^*}$, we arrive at the effective law of the wall predicted by k-ϵ and k-ω models, viz.,

$$u^+ \sim \frac{1}{\kappa}\ell n y^+ + B + \beta_T C\eta\ell n\eta \quad \text{as} \quad y^+ \to \infty \tag{25}$$

Figures 5 and 6 compare computed Launder-Sharma (LS) and baseline k-ω (WH) near-wall velocity profiles with experimental data, the standard law of the wall, and Eq. (25) for an equilibrium case (flow 2600) and a nonequilibrium case (flow 0141). In both cases the implied constant in the law of the wall B is 5.5 for the Launder-Sharma model and 5.0 for the k-ω model. As shown, the asymptotic formula provides an excellent approximation to the numerical results for all cases in the region between $y^+ = 20$ and 100. If we included the $\mathcal{O}(\eta^2\ell n\eta)$ term or used the exact defect-layer solution, the match would extend even farther above the sublayer. The important point to note is the impact of the term in Eq. (25) proportional to the equilibrium parameter β_T. In both of the cases shown, its effect is to distort the velocity profile throughout the defect layer, including its asymptotic form approaching the sublayer from above. This shows that the defect-layer perturbation solution applies, in a quasi-equilibrium sense, to nonequilibrium boundary layers. It also indicates that the k-ϵ model is incompatible with observed defect-layer structure of general turbulent boundary layers. Figures 5 and 6 show slight distortion of k-ω profiles for these two flows. This is a direct consequence of the small value of C relative to k-ϵ model values.

Table 4 Defect-layer coefficients

Model	$C_{\epsilon 1}$	$C_{\epsilon 2}$	C	κ
JL	1.45	2.00	13.06	0.46
LS	1.44	1.92	13.57	0.43
LB	1.44	1.92	13.57	0.43
CH	1.35	1.80	13.45	0.42
YS	1.44	1.92	13.57	0.43
FL	1.39	1.80	14.24	0.40
WH	—	—	2.90	0.41
WL	—	—	2.90	0.41

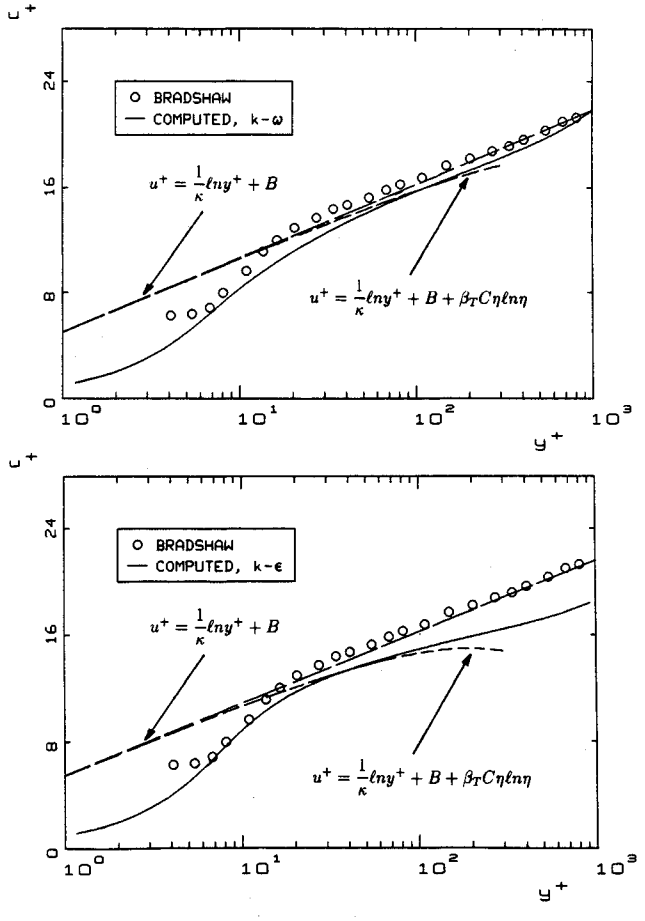

Fig. 5 Near-wall velocity profiles for flow 2600.

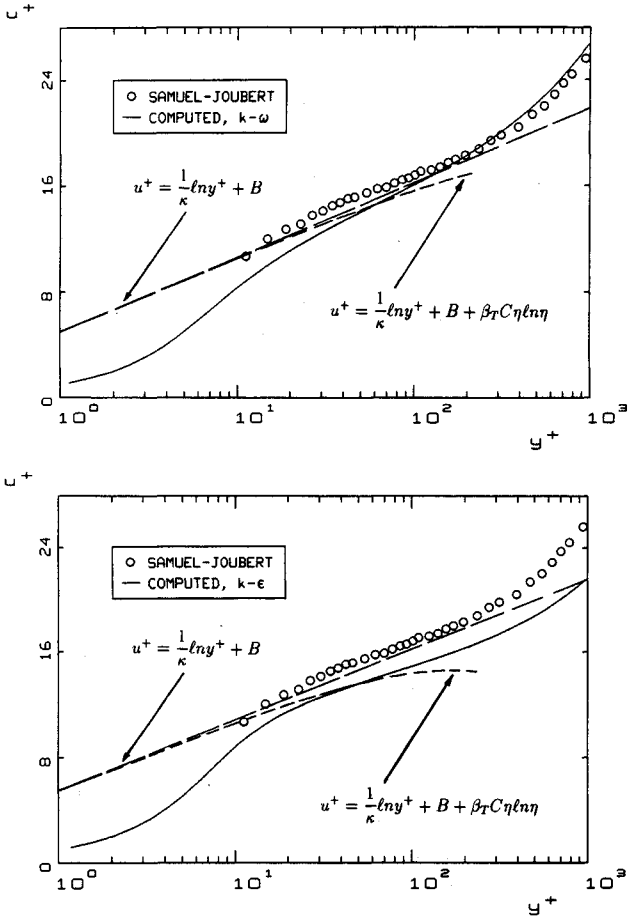

Fig. 6 Near-wall velocity profiles for flow 0141.

VI. Summary

Six low Reynolds number k-ϵ models, a high Reynolds number k-ω model, and a low Reynolds number k-ω model have been applied to 16 turbulent boundary layer flows. The applications include pressure gradients ranging from favorable to strong adverse, with one case very close to incipient separation. Results for all of the cases considered illustrate that viscous modifications are effective only well below the defect layer. The numerical results are entirely consistent with a perturbation analysis of the defect layer for both equilibrium and nonequilibrium boundary layers. The k-ϵ model's deficient defect-layer behavior dominates its predictions, which are satisfactory only for constant pressure and favorable pressure gradient. This further demonstrates the point made by Wilcox[6] that the k-ϵ model is very inaccurate in its description of the defect layer and is thus inconsistent with the dynamics of the turbulent boundary layer in a very fundamental way. By contrast, the k-ω model, without viscous corrections, is within acceptable engineering accuracy for all 16 flows. Including

k-ω viscous corrections produces almost identical results and even yields closer to measured skin friction for the nearly separated flow 5300.

References

[1]Jones, W. P., and Launder, B. E., "The Prediction of Laminarization with a Two-Equation Model of Turbulence," *International Journal of Heat and Mass Transfer,* Vol. 15, Feb. 1972, pp. 301–314.

[2]Launder, B. E., and Sharma, B. I., "Application of the Energy Dissipation Model of Turbulence to the Calculation of Flow Near a Spinning Disc," *Letters in Heat and Mass Transfer,* Vol. 1, No. 2, 1974, pp. 131–138.

[3]Chambers, T. L., and Wilcox, D. C., "Critical Examination of Two-Equation Turbulence Closure Models for Boundary Layers," *AIAA Journal,* Vol. 15, No. 6, 1977, pp. 821–828.

[4]Kline, S. J., Cantwell, B. J., and Lilley, G. M., *1980–81 AFOSR-HTTM-Stanford Conference on Complex Turbulent Flows,* Stanford Univ., Palo Alto, CA, 1981.

[5]Rodi, W., and Scheuerer, G., "Scrutinizing the k-ϵ Turbulence Model Under Adverse Pressure Gradient Conditions," *Transactions of the American Society of Mechanical Engineers,* Vol. 108, June 1986, pp. 174–179.

[6]Wilcox, D. C., "Reassessment of the Scale Determining Equation for Advanced Turbulence Models," *AIAA Journal,* Vol. 26, No. 11, Nov. 1988, pp. 1299–1310.

[7]Coles, D. E., and Hirst, E. A., *Computation of Turbulent Boundary Layers—1968 AFOSR-IFP-Stanford Conference,* Vol. II, Stanford Univ., Palo Alto, CA, 1969.

[8]Wilcox, D. C., "The Remarkable Ability of Turbulence Model Equations to Describe Transition," Fifth Symposium on Numerical and Physical Aspects of Aerodynamic Flows, California State Univ., Long Beach, CA, Jan. 13–15, 1992.

[9]Lam, C. K. G., and Bremhorst, K. A., "Modified Form of the k-ϵ-Model for Predicting Wall Turbulence," *Journal of Fluids Engineering,* Vol. 103, Sept. 1981, pp. 456–460.

[10]Chien, K.-Y., "Predictions of Channel and Boundary-Layer Flows with a Low-Reynolds-Number Turbulence Model," *AIAA Journal,* Vol. 20, No. 1, Jan. 1982, pp. 33–38.

[11]Yang, Z., and Shih, T.-H., "A New Time Scale Based k-ϵ Model for Near Wall Turbulence," *AIAA Journal,* Vol. 31, No. 7, pp. 1191–1198.

[12]Fan, S., Lakshminarayana, B., and Barnett, M., "A Low-Reynolds-Number k-ϵ Model for Unsteady Turbulent Boundary Layer Flows," *AIAA Journal,* (to be published).

[13]Wilcox, D. C., *Turbulence Modeling for CFD,* DCW Industries, Inc., La Cañada, CA, 1993.

[14]Blottner, F. G., "Variable Grid Scheme Applied to Turbulent Boundary Layers," *Computational Methods for Applied Mechanics and Engineering,* Vol. 4, No. 2, 1974, pp. 179–194.

[15]Wilcox, D. C., "Algorithm for Rapid Integration of Turbulence Model Equations on Parabolic Regions," *AIAA Journal,* Vol. 19, No. 2, 1981, pp. 248–251.

[16]Menter, F. R., "Influence of Freestream Values on k-ω Turbulence Model Predictions," *AIAA Journal,* Vol. 30, No. 6, 1992, pp. 1657–1659.

AIAA Education Series

Nonlinear Analysis of Shell Structures

A.N. Palazotto and S.T. Dennis

The increasing use of composite materials requires a better understanding of the behavior of laminated plates and shells for which large displacements and rotations, as well as, shear deformations, must be included in the analysis. Since linear theories of shells and plates are no longer adequate for the analysis and design of composite structures, more refined theories are now used for such structures.

This new text develops in a systematic manner the overall concepts of the nonlinear analysis of shell structures. The authors start with a survey of theories for the analysis of plates and shells with small deflections and then lead to the theory of shells undergoing large deflections and rotations applicable to elastic laminated anisotropic materials. Subsequent chapters are devoted to the finite element solutions and include test case comparisons.

The book is intended for graduate engineering students and stress analysts in aerospace, civil, or mechanical engineering.

1992, 300 pp, illus, Hardback, ISBN 1-56347-033-0, AIAA Members $47.95, Nonmembers $61.95, Order #:33-0 (830)

Place your order today! Call 1-800/682-AIAA

AIAA

American Institute of Aeronautics and Astronautics

Publications Customer Service, 9 Jay Gould Ct., P.O. Box 753, Waldorf, MD 20604
FAX 301/843-0159 Phone 1-800/682-2422 9 a.m. - 5 p.m. Eastern

Sales Tax: CA residents, 8.25%; DC, 6%. For shipping and handling add $4.75 for 1-4 books (call for rates for higher quantities). Orders under $100.00 must be prepaid. Foreign orders must be prepaid and include a $20.00 postal surcharge. Please allow 4 weeks for delivery. Prices are subject to change without notice. Returns will be accepted within 30 days. Non-U.S. residents are responsible for payment of any taxes required by their government.